Full-Particle Simulation of Electromagnetic Waves Induced by Electron Motion in a Field-Reversed Configuration*)

Takahiro URANO and Toshiki TAKAHASHI

Graduate School of Science and Technology, Gunma University, Kiryu 376-8515, Japan

(Received 27 December 2017 / Accepted 29 March 2018)

In this study, we perform full-particle simulation for field-reversed configuration plasma and observe fluctuations in the toroidal component of the electron current density. To verify the validity of the simulation, we examine the phase velocity of the vertical wave motion that exhibits several mesh sizes. Using spectrum analysis, we confirm that the peak of the oscillation power spectrum is close to the theoretical value of the electron plasma oscillation for an appropriate mesh size.

Keywords: field-reversed configuration, full-particle simulation, plasma frequency, fluctuation, phase velocity

DOI: 10.1585/pfr.13.3403055

1. Introduction

Field-reversed configuration (FRC) plasmas do not exhibit any toroidal magnetic field, and confinement can be achieved using a poloidal magnetic field that is generated by the plasma current in the toroidal direction [1]. The volume-averaged beta is given by $\langle\beta\rangle = 1 - 0.5x_s^2$ [2] with $x_s \equiv r_s/r_c$, where r_c is the coil radius and r_s denotes the separatrix radius. FRC plasmas exhibit a high beta with $\langle\beta\rangle = 0.875$ at $x_s = 0.5$. Additionally, because the plasma core region contains a field-null circle, the plasma size and ion radius are comparable. As a result, the finite Larmor radius effect contributes to the stability of FRC, and so far the deviation between MHD prediction and experimental observation has been considered as the research subject [3–5]. Although FRC plasma is a promising candidate that can be used as nuclear-fusion core plasma, the FRC generated by field-reversed theta-pinch method depicts a short lifetime of the order of 100 μs [1], and an improvement of the transport characteristics is essential for future applications. Given these considerations, in the C-2 experiment, the two FRCs are translated to obtain heating and remarkable improvement in the confinement [6]. Furthermore, as a result of the heating and current drive by Neutral Beam Injection (NBI) and the suppression of rotational instability due to the plasma gun, a dramatic improvement has been achieved in terms of the plasma performance [7]. The improvement in transport properties can be attributed to ions with large Larmor radius that is comparable with the plasma size; such ions are known as betatron particles [8]. Further, an attempt to understand the transport properties of the bulk plasma, excluding the beam component, has led to further developments. The initial plasma current can be almost completely attributed to the diamagnetic current of electrons, and it is inevitable that the contribution of the electron fluid to the fluctuating component of the confining magnetic field will become significant. Although frequency values that are up to several tens of MHz have been observed in various experiments, no experiments have been conducted to investigate the relation between the high frequency fluctuations and the properties of the electron fluid. Given the recent improvements in computing, it has become feasible to develop research infrastructure to clarify the electronic behavior in the high-beta plasmas. In this study, we construct a simulation model of electromagnetic fluctuations based on the electron motion in high-beta FRC plasma. We consider a case of highly inhomogeneous magnetic field and discuss its numerical characteristics. To summarize, the objective of our study is to clarify the properties of the electronic-fluid fluctuation field in FRC.

2. Simulation Model

2.1 Simulation region and equilibrium state

The simulation target is the Nihon University Compact Torus Experiment (NUCTE)-III [9] device at Nihon University. The coordinate system is a two-dimensional cylindrical coordinate system assuming axisymmetry. Figure 1 depicts the simulation region and initial density. We use half of the FRC cross-section to be the simulation region. The initial pressure and magnetic distributions are chosen to be the solutions of the Grad–Shafranov equation. The initial temperature distribution model is assumed to be constant within the separatrix with electron temperature $T_e = 50$ [eV] and ion temperature $T_i = 100$ [eV]. The distribution is assumed to be gradually decreasing outside the separatrix. Figure 2 depicts the z component of the magnetic field and the plasma pressure at the midplane in the equilibrium state. To reproduce the initial electron flow ve-

author's e-mail: t-tak@gunma-u.ac.jp

*) This article is based on the presentation at the 26th International Toki Conference (ITC26).

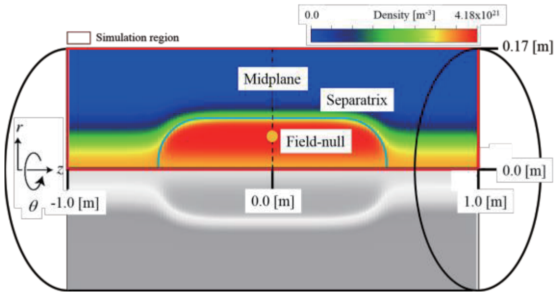

Fig. 1 Simulation region.

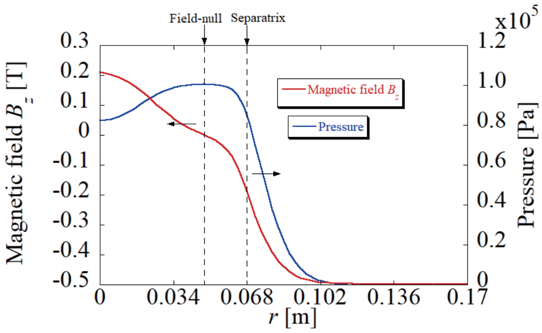

Fig. 2 z component of the magnetic field and the plasma pressure at the midplane in an equilibrium state.

locity, we assumed that only the toroidal velocity component can be described by the shifted Maxwell distribution, whereas the remaining two components can be given by the conventional non-shifted Maxwellian. Further, the initial ion-flow velocity is assumed to be zero. Consequently, the initial electric field is observed to be dependent on the ion pressure gradient.

2.2 Full-particle simulation equations

The following ((1) - (3)) formulas were used to perform the field calculation:

$$\mathbf{j} = qn_\mathrm{i}\mathbf{u}_\mathrm{i} - en_\mathrm{e}\mathbf{u}_\mathrm{e}, \tag{1}$$

$$\frac{\partial \mathbf{E}}{\partial t} = c^2(\nabla \times \mathbf{B}) - \frac{\mathbf{j}}{\varepsilon_0}, \tag{2}$$

$$\frac{\partial \mathbf{B}}{\partial t} = -\nabla \times \mathbf{E}, \tag{3}$$

where $\mathbf{j}$ denotes the current density, q and e denote the ion and elementary charges, n_i and n_e denote the ion and electron densities, $\mathbf{u}_\mathrm{i}$ and $\mathbf{u}_\mathrm{e}$ denote the ion and electron flow velocities, $\mathbf{E}$ denotes the electric field, t denotes the time, c denotes the light speed, ε_0 denotes the permittivity of vacuum, and $\mathbf{B}$ denotes the magnetic field. The Euler method is used to perform time differentiation in Eqs. (2) and (3). The physical quantities $\mathbf{u}_\mathrm{i}$, $\mathbf{u}_\mathrm{e}$, n_i, and n_e are obtained by tracking the trajectories of ions and electrons using calculations that employ the particle-in-cell (PIC) method.

The initial ions and electrons are uniformly loaded into the cells across the calculation area as 'super particles' that exhibit statistical weights, which can be defined by the Maxwell distribution as follows:

$$f_{M\mathrm{i,e}} = n_\mathrm{i,e}\left(\frac{m_\mathrm{i,e}}{2\pi T_\mathrm{i,e}}\right)^{3/2} \exp\left(-\frac{m_\mathrm{i,e}v_\mathrm{i,e}^2}{2T_\mathrm{i,e}}\right), \tag{4}$$

where $v_\mathrm{i,e} = \sqrt{v_r^2 + v_\theta^2 + v_z^2}$ is the speed of ions or electrons, $m_\mathrm{i,e}$ is the ion or electron rest mass, and $T_\mathrm{i,e}$ is the ion or electron temperature. The motion of particles is calculated using the relativistic equations of motion as follows:

$$\frac{\mathrm{d}(\gamma m_\mathrm{i,e}\mathbf{v}_\mathrm{i,e})}{\mathrm{d}t} = q_\mathrm{i,e}(\mathbf{E} + \mathbf{v}_\mathrm{i,e} \times \mathbf{B}), \tag{5}$$

$$\gamma = \frac{1}{\sqrt{1-(v_\mathrm{i,e}^2)/c^2}}, \tag{6}$$

where $q_\mathrm{i,e}$ is the ionic or electron charge ($q_\mathrm{e} = -e$ where e is the elementary charge) and γ is the Lorentz factor. Although relativistic equations are used here for the sake of caution, the Lorentz factor is almost 1 in the calculation targeted in this study, and it can be handled classically. Here, we adopt a collisionless model; further, because the electron mass is assumed to be as it is, the ion-to-electron mass ratio for deuterium ions is observed to be approximately 3,672.

3. Results and Discussion

To establish the validity of our simulations, we performed the full-particle simulations in case of four patterns of meshes, $N_r \times N_z = 33 \times 65$, 65×129, 129×257, and 257×512, where N_r and N_z denote the mesh sizes in both r and z directions. In our calculations, the particle number changed according to the density of a mesh to secure a sufficient number of super-particles within one cell.

For $N_r \times N_z = 129 \times 257$, the obtained radial profiles are depicted in Figs. 3 - 5. No time change is observed in the ion and electron densities or in the z component of the magnetic field, as depicted in Figs. 3 and 4.

Figure 5 presents the radial profiles of the θ component of the electron-flow velocity as well as its fluctuation component. This result indicates that fluctuations in the flow velocity occurred. A relatively large change is observed in the electron-flow velocity in the vicinity of the separatrix at 42.3 [ps]. The effects of ions can be ignored in this simulation because the change in the ion-flow velocity is observed to be approximately four orders of magnitude smaller than that in the electron flow velocity.

For simulation validity check, we discuss the phase velocity of the waves that were caused due to the fluctuations generated near the separatrix by varying the mesh size. Figure 6 depicts the time dependence of the fluctuations at the midplane. The waves generated in the vicinity of the separatrix are observed to gradually propagate toward the inner region of the FRC plasma, which allows us to estimate the phase velocity.

The result is depicted by orange points in Fig. 7. The phase velocity converges toward the light velocity as the

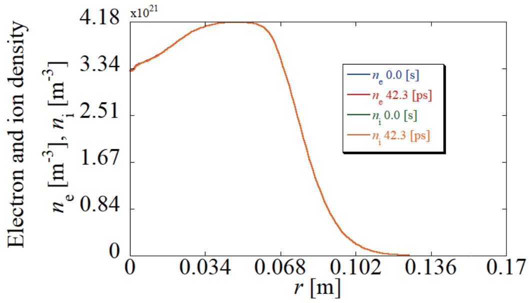

Fig. 3 Time evolution of the ion and electron densities at the midplane.

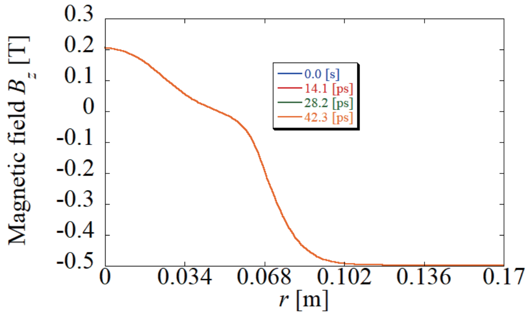

Fig. 4 Time evolution of the z component of the magnetic field at the midplane.

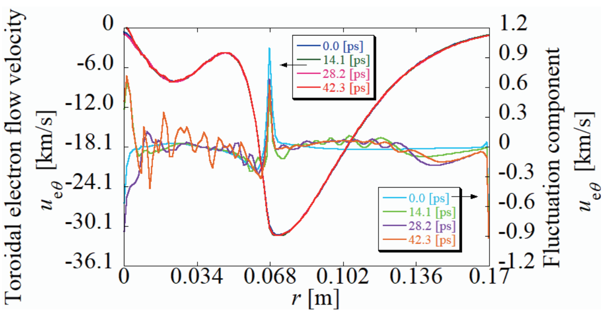

Fig. 5 Time evolution of $u_{e\theta}$ at the midplane.

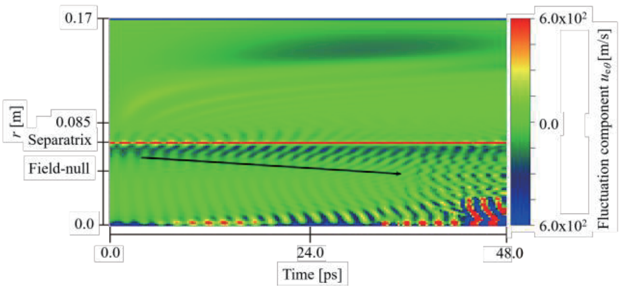

Fig. 6 Time change of fluctuation.

mesh becomes denser. To investigate the effect of the mesh size on the phase velocity, we discuss the dispersion relation using a virtual wavenumber that should be considered due to the limited spatial resolution. Because this

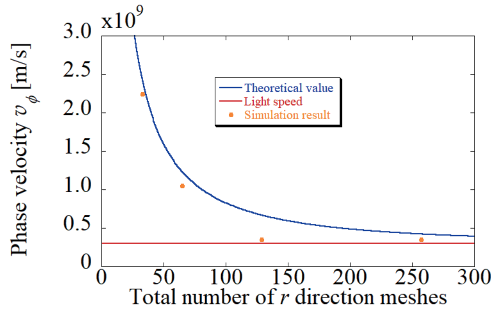

Fig. 7 Relation between the phase velocity and the mesh size.

wave propagates perpendicularly to the magnetic field, we should consider the dispersion relation of the transverse wave. However, because FRC is described by a weak magnetic field and high density, the frequency of plasma oscillations is observed to exceed that of the cyclotron oscillation. The electron cyclotron frequency and plasma oscillation frequency at the midplane and separatrix are $\omega_{ce} = 3.79 \times 10^{10}$ [Hz] and $\omega_{pe} = 3.27 \times 10^{12}$ [Hz], respectively. The plasma oscillation is two orders of magnitude larger than the cyclotron oscillation. Therefore, we consider that the cyclotron oscillation can be neglected. Therefore, the discussion below assumes a regime with no dc magnetic field [10]. Therefore, the dispersion relation can be approximated as

$$\omega^2 = \omega_p^2 + c^2k^2, \tag{7}$$

and the corresponding phase velocity can be given as

$$v_\phi = \frac{\omega}{k} = \sqrt{\frac{\omega_p^2}{k^2} + c^2}. \tag{8}$$

This approaches the speed of light as the artificial wavenumber, k, increases. Because the wavenumber depends on the mesh density, we set $k = AM$, where A is the proportionality constant and M is the size of the mesh. In this case, we used A as the reciprocal of the distance between the field-null and separatrix. We observe that there is a good agreement with the simulation results, as illustrated by the blue line in Fig. 7, suggesting that the full particle simulation of FRC is appropriately performed in the calculation where the mesh is larger than $N_r \times N_z = 129 \times 257$.

In this manner, we present the results that were obtained using a mesh of size $N_r \times N_z = 129 \times 257$. We present the oscillatory time dependence of the electron flow velocity, $u_{e\theta}$, at the separatrix and field-null on the midplane in Fig. 8. During the early stage of simulation, the amplitude of $u_{e\theta}$ at the separatrix is observed to be larger than the value at the field-null. The amplitude at the separatrix decreases after approximately 20 [ps] and increases again from approximately 40 [ps]. However, at the field-null, the electron velocity begins to increase at 20 [ps] and experiences further increase at approximately 30 [ps]. The increase in amplitude may be caused due to

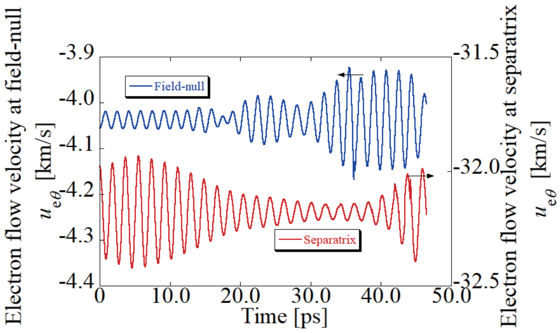

Fig. 8 Time evolution of $u_{e\theta}$ at the field-null and separatrix.

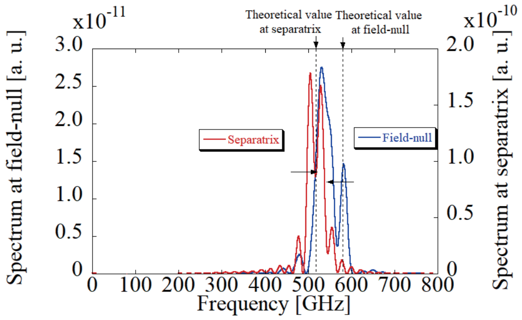

Fig. 9 The result of Fourier analysis of the electron flow velocity at the field-null.

electromagnetic fluctuations and particle interactions. The detailed analysis of this behavior is remaining, and this can be performed in a future study.

We have performed the Fourier transform of $u_{e\theta}$ to obtain the power spectrum of the oscillations. The results are presented in Fig. 9. The Fourier transformation was performed after cutting off the direct current component of the electron flow velocity, $u_{e\theta}$.

We note that the peak value of the spectrum in Fig. 9 is close to the theoretical value of plasma oscillations, which indicates that the oscillations that have been observed in our simulations are electron plasma oscillations. In the model that has been considered in our study, the ion flow velocity is negligibly small as compared to the electron flow velocity. Therefore, the current density is determined using the electron flow velocity. However, the electromagnetic field changes with current density as a source. Therefore, the electromagnetic field is also observed to oscillate at the same frequency as that of the electron plasma oscillations.

4. Summary

We performed a full particle simulation of FRC and calculated the electronic fluid fluctuation field. The simulation time was 48 [ps], and we were able to observe the electron plasma oscillations. During the initial stage of the calculation, the fluctuations were observed to be large near the separatrix. They propagated toward the inner region of FRC plasma with the phase velocity of the speed of light.

The future work is to clarify the relation between the electron fluid fluctuation field and particle transport by further long time calculation.

Acknowledgment

This work is performed on “Plasma Simulator” (FUJITSU FX100) of NIFS with the support and under the auspices of the NIFS Collaboration Research program (NIFS15KNST087).

[1] M. Tuszewski, Nucl. Fusion **28**, 2033 (1988).
[2] D.C. Barnes *et al.*, in Compact Toruses and Energetic Particle Injection (Proc. US-Japan Joint Symp. Princeton, NJ, 1979), PPPL, Princeton University (1979) 110.
[3] N. Iwasawa *et al.*, Phys. Plasmas **8**, 1240 (2001).
[4] E.V. Belova *et al.*, Phys. Plasmas **8**, 1267 (2001).
[5] Yu. A. Omelchenko, Phys. Plasmas **7**, 1443 (2000).
[6] M.W. Binderbauer *et al.*, Phys. Rev. Lett. **105**, 045003 (2010).
[7] M. Tuszewski *et al.*, Phys. Plasmas **19**, 056108 (2012).
[8] L. Schmitz *et al.*, Nature Communications **7**, 13860 (2016).
[9] T. Asai *et al.*, Phys. Plasmas **13**, 072508 (2006).
[10] F.F. Chen, *Introduction to Plasma Physics* (Plenum Press, New York, 1974) p.102.